electronic reprint

JOURNAL OF APPLIED CRYSTALLOGRAPHY

ISSN: 1600-5767
journals.iucr.org/j

SAS-cam: a program for automatic processing and analysis of small-angle scattering data

Hongjin Wu, Yiwen Li, Guangfeng Liu, Haiguang Liu and Na Li

J. Appl. Cryst. (2020). **53**, 1147–1153

IUCr Journals
CRYSTALLOGRAPHY JOURNALS ONLINE

Copyright © International Union of Crystallography

Author(s) of this article may load this reprint on their own web site or institutional repository provided that this cover page is retained. Republication of this article or its storage in electronic databases other than as specified above is not permitted without prior permission in writing from the IUCr.

For further information see https://journals.iucr.org/services/authorrights.html

JOURNAL OF APPLIED CRYSTALLOGRAPHY

ISSN 1600-5767

SAS-cam: a program for automatic processing and analysis of small-angle scattering data

Hongjin Wu,[a,b] Yiwen Li,[a] Guangfeng Liu,[a] Haiguang Liu[c]* and Na Li[a]*

[a]National Facility for Protein Science in Shanghai, Zhangjiang Laboratory, Shanghai Advanced Research Institute, Chinese Academy of Sciences, No. 333 Haike Road, Shanghai 201204, People's Republic of China, [b]CAS Key Laboratory of Molecular Virology and Immunology, Institute Pasteur of Shanghai, Chinese Academy of Sciences, No. 320 Yueyang Road, Shanghai 200031, People's Republic of China, and [c]Complex Systems Division, Beijing Computational Science Research Center, 8 E Xibeiwang Road, Haidian, Beijing 100193, People's Republic of China. *Correspondence e-mail: hgliu@csrc.ac.cn, nli@sibcb.ac.cn

Received 6 May 2020
Accepted 1 July 2020

Edited by F. Meilleur, Oak Ridge National Laboratory, USA, and North Carolina State University, USA

Keywords: small-angle scattering; data processing; automated pipelines; synchrotrons; high-throughput experiments.

Small-angle X-ray scattering (SAXS) is a widely used method for investigating biological macromolecules in structural biology, providing information on macromolecular structures and dynamics in solution. Modern synchrotron SAXS beamlines are characterized as high-throughput, capable of collecting large volumes of data and thus demanding fast data processing for efficient beamline operations. This article presents a fully automated and high-throughput SAXS data analysis pipeline, *SAS-cam*, primarily based on the *SASTBX* package. Five modules are included in *SAS-cam*, encompassing the data analysis process from data reduction to model interpretation. The model parameters are extracted from SAXS profiles and stored in an HTML summary file, ready for online visualization using a web browser. *SAS-cam* can provide the user with the possibility of optimizing experimental parameters based on real-time feedback and it therefore significantly improves the efficiency of beam time. *SAS-cam* is installed on the BioSAXS beamline at the Shanghai Synchrotron Radiation Facility. The source code is available upon request.

1. Introduction

Small-angle X-ray scattering (SAXS) is a useful low-resolution method in structural biology research, playing an important complementary role to high-resolution structure determination methods. The wide applications of SAXS arouse continually growing interest within the biological science research community (Jacques & Trewhella, 2010; Graewert & Svergun, 2013). The recent progress in synchrotron facilities and SAXS instruments has made SAXS data collection highly automated with high-throughput operations (Hura *et al.*, 2009; Blanchet & Svergun, 2013; Liu *et al.*, 2018). This trend is reflected in the fast-growing application of the SAXS method in characterizing the structures of homogeneous biological macromolecules in solution (Rodríguez-Ruiz *et al.*, 2017) and heterogenous molecular systems (Kim *et al.*, 2020).

Considering the large quantities of data being collected with advanced instruments that support high repetition rates, efficient usage of synchrotron beamlines becomes a critical issue to the synchrotron user community (Pandolfi *et al.*, 2018). Several state-of-the-art software packages have been developed to analyse biological SAXS data, such as *ATSAS* (Franke *et al.*, 2017), *SASTBX* (Liu *et al.*, 2012) and *BioXTAS RAW* (Nielsen *et al.*, 2009). In spite of the advances in software development, a highly integrated automated data processing and analysis tool is an indispensable prerequisite for efficient beamline operations.

© 2020 International Union of Crystallography

electronic reprint

At the Shanghai Synchrotron Radiation Facility, the biological small-angle X-ray scattering (BioSAXS) beamline BL19U2 (Li *et al.*, 2016; Liu *et al.*, 2018) was recently upgraded with a high-throughput robotic sample loader to facilitate efficient scattering data collection. The full automation of a scattering experiment also requires efficient data analysis. To cope with the demand of the large volumes of data that are collected in a high-throughput experiment, the data analysis pipeline *SAS-cam* has been implemented and integrated on the BL19U2 beamline. The pipeline is mainly coded in Python with the consideration of high portability and expandability. The prerequisite packages were kept within standard libraries, such as NumPy (https://numpy.org/), SciPy (https://www.scipy.org/) and PIL (http://www.pythonware.com/products/pil/), which are utilized to handle SAXS data processing (such as 2D scattering pattern visualization, or 1D radial profile calculation). A data integration program has been developed to obtain 1D scattering profiles in batch mode. After integrating the experimental scattering patterns to SAXS profiles, the subsequent data interpretation is carried out using modules in the *SASTBX* package (Liu *et al.*, 2012).

SAS-cam has been deployed on the BL19U2 beamline and is used as an automated SAXS data processing pipeline, covering the major data analysis procedures for standard SAXS experiments. *SAS-cam* is a platform for processing the scattering data obtained from automated sample-loading systems (Liu *et al.*, 2018). Currently, *SAS-cam* includes five modules: (i) an integration module that reduces 2D scattering patterns to 1D scattering curves; (ii) a data comparison and averaging module to obtain the average SAXS profile after filtering out the outliers on the basis of profile similarity; (iii) a background subtraction module, scaling and subtracting the background scattering from the total scattering signal to obtain the SAXS profile corresponding to the density contrast between the sample molecules and buffer; (iv) an analysis module, determining the overall structural parameters and low-resolution 3D models; and (v) a result rendering module, summarizing the results for interactive visualization.

2. Features

The *SAS-cam* program can be launched from a terminal using a command line and, once started, it will run with full automation. Fig. 1 shows the workflow of *SAS-cam*.

This data analysis pipeline provides an efficient data reduction module, mainly based on modules in standard libraries such as NumPy and PIL. The workflow contains five modules that are triggered automatically by new experimental data. The workflow starts with handling 2D scattering patterns and finishes with the construction of low-resolution models. Briefly, the 2D scattering patterns recorded on the X-ray detectors are radially averaged by the integration module. Data averaging of a number of frames (typically 20 frames in batch mode) is cross compared to detect radiation damage using a correlation map (Franke *et al.*, 2015) by the data comparison and averaging module. The buffer scattering is subtracted from the sample signal with a sample concentration normalization by the background subtraction module. Further analyses of the SAXS data after background subtractions, such as Guinier approximation (Guinier & Fournet, 1955), molecular mass estimation, pair distance distribution function $P(r)$ and particle shape reconstructions, are completed by the analysis module. The derived model parameters and 3D models are stored in an HTML summary file which is generated by the result rendering module.

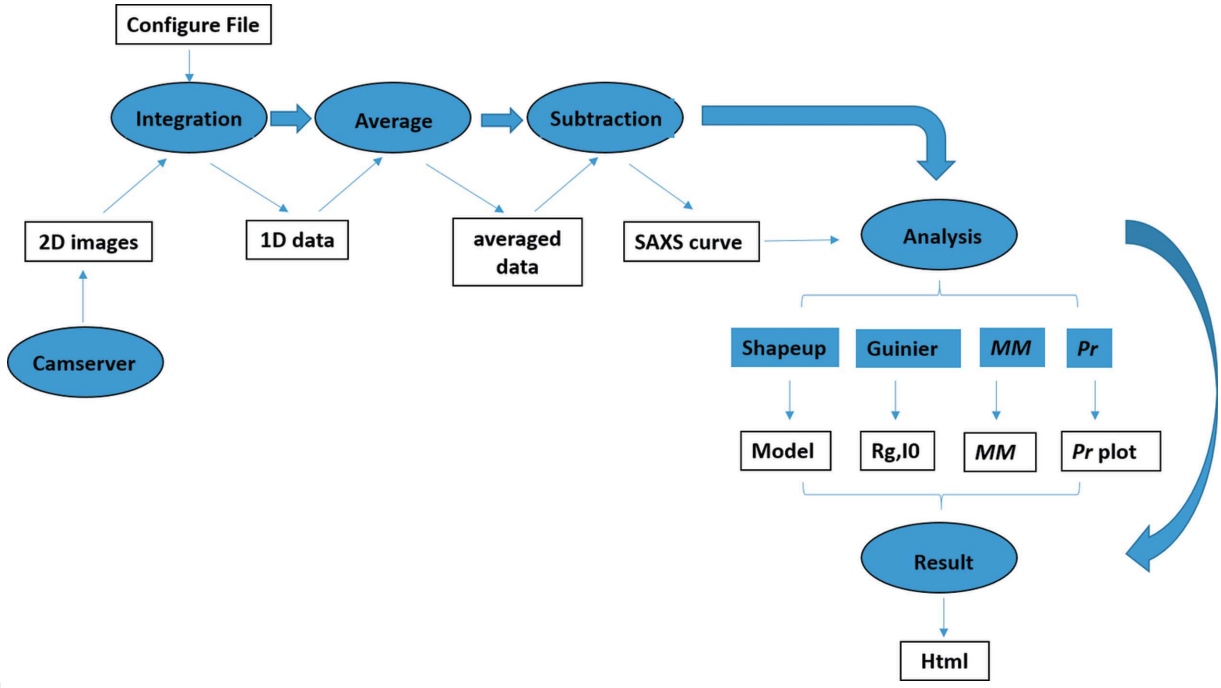

Figure 1
Workflow of the *SAS-cam* pipeline implemented on the BL19U2 beamline.

electronic reprint

3. Modules

3.1. Integration module

The PIL library is used to decode 2D scattering images from TIF format into the corresponding data array in the NumPy format. The data averaging can be processed with a throughput of 200–250 frames per minute for TIF images composed of 981 × 1043 pixels with a standard single-processor computer (Intel Core i5-4210U CPU @ 2.40 GHz). A configuration file should be prepared, based on a template file for radial averaging. The configuration file contains mask information (an image file with marked detector gaps and bad pixels) and scattering data collection instrumental information (*e.g.* beam energy, sample-to-detector distance, beam centre *etc.*). This configuration file is compatible with the *BioXTAS RAW* program (Hopkins *et al.*, 2017). Therefore, relevant source code originating from *BioXTAS RAW* is included in this module. The output of this module is the standard SAXS profile format composed of three columns (q, i and σ), where q is the momentum transfer [$q = 4\pi\sin\theta/\lambda$, with 2θ the scattering angle and λ the wavelength], i is the scattering intensity and σ is the standard deviation. The header of the scattering profile complies with the format suggested by the Small-Angle Scattering Biological Data Bank (Kikhney *et al.*, 2020). An example header is given in Table 1.

A flowchart of the radial averaging operation in *SAS-cam* is summarized in Fig. 2. The positions of the pixels are mapped to q values in reciprocal space on the basis of the instrumental setup and X-ray parameters. Each pixel on the 2D X-ray detector is mapped to a q value, and these are further binned to discretized q arrays. To facilitate the calculation, both pixel and q-value matrices are reshaped to 1D arrays. The pixels are grouped according to the corresponding q values, which are converted to q indices by rounding $q/q_{\rm step}$ to the nearest integer values of the q indices (where $q_{\rm step}$ determines the sampling rate in the final SAXS profile). Pixels with the same q indices are grouped and saved in a list for future use. After the mapping operation, each list contains pixel indices with q values between q and $q + q_{\rm step}$. Pixels in the masked regions are excluded from the index lists. For example, the first list contains pixels whose q values are in the range from $q_{\rm min}$ to $q_{\rm min} + q_{\rm step}$ ($q_{\rm min}$ is the minimum momentum transfer that can be measured for a given experimental setup). For each experimental setup, this mapping operation needs to be executed once, prior to the radial profile calculations. When integrating an experimental scattering pattern (reshaped to one dimension), the average values and standard deviations are calculated for each list, and then gathered to obtain the 1D integrated profile and its associated standard deviations.

Table 1
Illustration of the header section in the integrated scattering profile.

Instrument	BL19U2
Detector	Pilatus 1M
Date	2019-12-04
Wavelength (nm)	0.124
Sample-to-detector distance (m)	2.01
Exposure time per frame (s)	1.0

3.2. Data comparison and average module

In a standard data collection process, a set of scattering patterns will be collected for each measurement condition. Patterns in the same batch may differ from each other, due to measurement errors and systematic errors, including fluctuations in the X-ray beam. Therefore, during data processing, differences within the batch of scattering curves corresponding to the same measurement condition should be analysed and outliers should be excluded from further analysis. The CorMap method proposed by Franke *et al.*

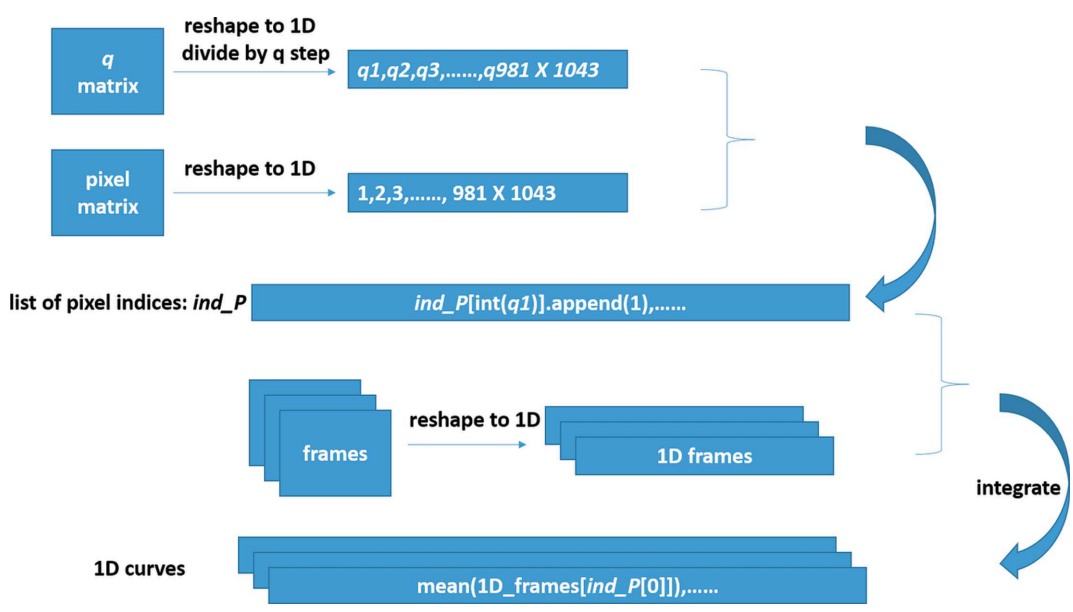

Figure 2
Illustration of the radial averaging workflow.

electronic reprint

(2015) is used to compare 1D SAXS data, as a component in the *SAS-cam* pipeline. The underlying principle for CorMap is that the distribution of a scattering curve satisfies the n-variate normal distribution. Therefore, the correlation matrix (or correlation map) for any two scattering curves can be calculated. For two similar curves, points from the two curves at different angles are independent of one another, resulting in random numbers in the correlation map [shown in Fig. 3(*b*)]. For two curves that are significantly different, the corresponding correlation map contains contiguous areas [shown in Fig. 3(*d*)]. This feature can be used to compare curves and select similar curves from the data set. After analysing the correlation map for a large quantity of data, it was found that the edge length of the largest contiguous region satisfied the distribution of the longest head-or-tail runs in a coin-toss experiment (Schilling, 1990). If the statistical significance P is smaller than a threshold α, the difference between the data curves is considered to be significant. Scattering curves without a significant difference are averaged to get the 1D profile for further analysis. For example, the SAXS data sets shown in Fig. 3(*a*) have high similarities and all 20 data frames are averaged. However, only six of the data frames shown in Fig. 3(*c*) are selected and averaged on the basis of the CorMap output. Data frames measured on potentially damaged samples are excluded from further analysis. In *SAS-cam*, the

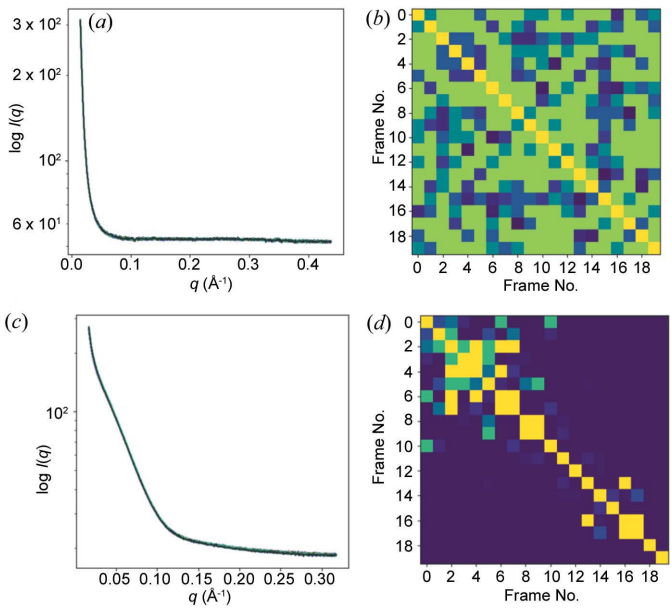

Figure 3
CorMap illustration. (*a*), (*c*) One-dimensional SAXS data sets, each consisting of 20 data frames, collected from (*a*) aqueous buffer and (*c*) bovine serum albumin (BSA) with accumulated radiation damage (unsubtracted data). (*b*), (*d*) CorMaps for the 1D experimental data comparison. The corresponding probabilities of similarity (P value) for the ith and jth frames on the matrix are shown by the colour of the pixel; a brighter colour means a higher similarity ($P \simeq 1$). Points on the diagonal line are of the highest brightness with $P = 1$. (*b*) The CorMap for the buffer profiles shows high similarity and all 20 data frames can be used for averaging. (*d*) The BSA sample profiles show variations in similarity, which are attributed to accumulated radiation damage. *SAS-cam* can automatically compare data from 20 measurements and only the first six frames with high similarity are used for profile averaging.

predetermined significance level α is set to $P > 0.01$. The source code of CorMap is from the *Freesas* program (https://github.com/kif/freesas) developed by Jerome Kieffer.

3.3. Background subtraction module

The background subtraction module was developed to remove the buffer contribution from the total scattering signal. For every sample profile, the module automatically searches the data set to find all the matched buffer profiles according to the code flag marked in the header file. For each sample measurement, the closest buffer measurement is taken as the matched buffer data based on the time stamps saved in the header section. The background subtraction profile is scaled on the basis of the transmitted beam intensities recorded in a separate file in ASCII text format. The scaling factor is given by

$$\beta = I_{\rm s}/I_{\rm b}, \qquad (1)$$

where β is the scaling coefficient and $I_{\rm s}$ and $I_{\rm b}$ are the transmitted beam intensities for sample and buffer, respectively. Note that *SAS-cam* automatically normalizes the scattering intensity on the basis of the measured transmitted beam intensity. Calibration with absolute intensity standard SRM 3600 (NIST, USA) and water is not yet included in *SAS-cam*.

3.4. Analysis module

Once the above data reduction procedures are completed, a SAXS profile corresponding to the density contrast between sample molecules and displaced buffer will be ready for detailed analysis. The analysis module includes four main functions, namely shape retrieval from a model database, Guinier analysis, molecular mass estimation and $P(r)$ calculation. The *sastbx.shapeup* program in the *SASTBX* package is used to retrieve molecular shapes from the shape database generated from known macromolecular complexes (Liu *et al.*, 2012). Ten candidate 3D shapes whose model profiles best match the experimental SAXS data are retrieved and constructed.

The Guinier analysis is carried out with a linear fitting of $\log(I)$ to q^2 for a window within the Guinier region [$q_{\rm min}$, $1.0/R_{\rm g}$] where $R_{\rm g}$ is the radius of gyration. The fitting region is optimized to get the best linear fit by sliding the data window and varying its length. The slope is used to infer $R_{\rm g}$, while the extrapolated intercept on the y axis [$\log(I)$] is used to determine $I(0)$. The $P(r)$ function is approximated using an analytical function in the following parametric form:

$$P(r) = g(r)\,\exp\left[\sum_{n=0}^{N} a_n\, T_n\left(\frac{2r}{D_{\rm max}} - 1\right)\right], \qquad (2)$$

where $g(r)$ is the $P(r)$ of a sphere of maximum dimension $D_{\rm max}$ to ensure the boundary conditions [$P(0)$ and $P(D_{\rm max})$ are both 0]. a_n and $T_n(r)$ are the weighting coefficient and Chebyshev polynomial of degree n, respectively. $P(r)$ was converted to a SAXS profile via the Debye formula for direct comparison with the experimental data. Optimization of the coefficients $\{a_n\}$ with the target of minimizing the χ score between model

electronic reprint

and experimental SAXS profiles will yield the desired $P(r)$ function for a given D_{max}. There is an option in the $P(r)$ function calculation to locate the optimal D_{max} in the neighbourhood of a given value (Liu & Zwart, 2012).

The molecular mass (MM) determination routine estimates the sample MM in comparison with standard proteins of known MM. The method used in *SAS-cam* is described by the following equation:

$$M = \frac{I_{0_ref}\, c_{ref}\, M_{ref}}{I_0\, c}, \qquad (3)$$

where I_{0_ref}, c_{ref} and M_{ref} are the scattering intensity at zero angle, the solution concentration and the MM of the standard protein, respectively, and I_0, c and M are the scattering intensity at zero angle, concentration and MM of the measured protein, respectively.

The 3D shapes are obtained via a fast shape retrieval approach, with an automated model size optimization to match experimental SAXS profiles. The precompiled shape database is composed of diverse shapes obtained from protein databases. The shapes are scaled to fit optimally inside a unit sphere (*i.e.* $r = 1.0$). During the shape retrieval procedure, the shapes are scaled to the desired radius, which is optimized to get the best fit to the experimental SAXS profile. By default, ten models with the best matched SAXS profiles are retrieved and the electron densities are constructed. The ten models are grouped according to their similarity to cross check the internal model consistency. For monodisperse samples and high-quality SAXS data, the retrieved models are highly similar. If multiple groups are obtained for the ten models, the user is advised to check the sample quality and measurement conditions to avoid sample heterogeneity or aggregation.

3.5. Result rendering module

For a large number of measurements in each batch experiment, it is important to compare the outcomes by summarizing and displaying the results in an organized document. This is achieved by applying the result rendering module, which collects the outputs and organizes them into a table that can be displayed on a web server hosted on the data-processing computer. For each experiment with many measurements (for the same sample or different samples), the result rendering module dynamically creates a web page showing a summary of the analysis results. The web page includes the following information: D_{max} (maximum dimension of the molecule), MM, R_g, $I(0)$ and a low-resolution 3D model. This routine was based on the *pyH* package (https://code.google.com/archive/p/pyh/). The *Jmol* applet (http://www.jmol.org/) is used to display the molecular models in a web page to allow interactive visualizations.

4. Examples

SAS-cam can be initiated via a single command, `sastbx.python SAS_cam.py`. A configuration file is needed before executing the start command to assign the paths to locate the 2D image files and to save 1D profiles. An illustration of a configuration file is given in Fig. 4.

The performance of *SAS-cam* has been tested on the BL19U2 beamline using the standard proteins bovine serum albumin (BSA) and lysozyme. Fig. 5 shows the results for BSA viewed using the Firefox web browser.

In the web browser, a table shows the sample name, D_{max}, R_g, $I(0)$, MM and the averaged 3D model in six columns. As more measurements are added, the table will be updated by appending the new results to the bottom row. For the standard protein BSA (Sigma, product No. A7030), the *SAS-cam* output shows a good agreement with the standard values for BSA with a small amount of aggregation, as confirmed in the heterogeneity measurement using size-exclusion column (SEC)-SAXS (shown in Fig. 6). This explains why the calculated MM for BSA is slightly higher than that of the BSA monomer ($MW_{monomer,\,BSA}$ = 67 kD). The instrumentation details for the SEC-SAXS mode can be found in our previous work (Liu *et al.*, 2018). In general, BSA solution (~150 µl, 5 mg ml^{-1}) was injected into the high-performance liquid chromatography system and purified through the column

```
#########################################
# Configure file for the sas-cam pipeline #
#########################################

import os

image_dir = '/home/hongjin/data/bsa/images'
base_dir = '/home/wuhj/data/bsa_saxs2_20191204'
cfg = "/home/wuhj/cfg/20151112.cfg"
RAW_dir = "/home/wuhj/software/RAW"

ref_MW = 70
ref_I0 = 213
ref_Conc = 4.5

txt_dir = image_dir
dat_dir = os.path.join(base_dir,'1D')
aver_dir = os.path.join(base_dir,'aver')
sub_dir = os.path.join(base_dir,'sub')
pr_dir = os.path.join(base_dir,'pr')
model_dir = os.path.join(base_dir,'model')
guinier_dir = os.path.join(base_dir,'guinier')
```

Figure 4
Illustration of the configuration file for *SAS-cam* on the BL19U2 beamline.

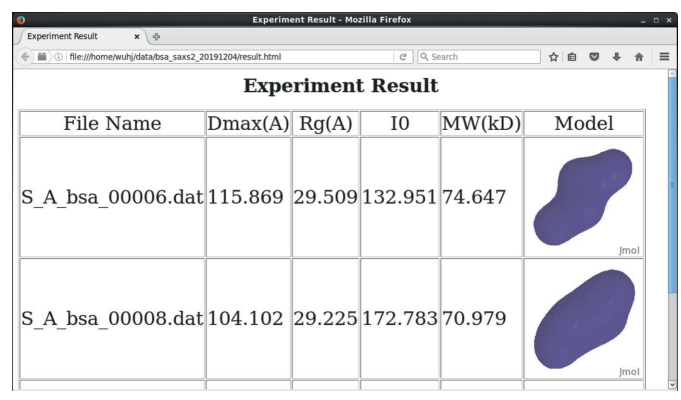

Figure 5
Illustration of *SAS-cam* performance with the standard protein BSA.

electronic reprint

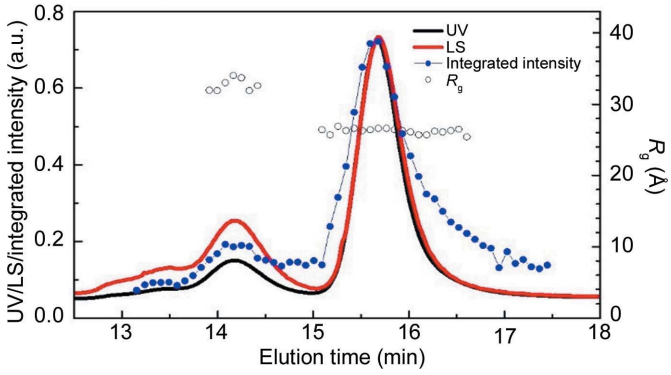

Figure 6
Inline SEC-SAXS measurement for BSA on the BL19U2 beamline. The multiple peaks indicate the heterogeneity of the BSA samples being tested.

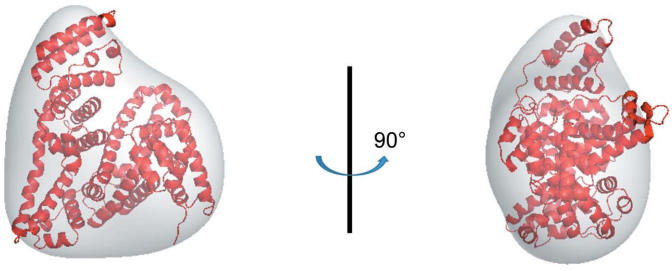

Figure 7
Superimposition of the SAXS envelope (grey surface) with the crystal structure of BSA (red cartoon).

(24 ml Superdex-200 Increase, GE Healthcare). At the exit of the column, the eluent is successively pumped through UV absorption and multi-angle static light scattering (LS) detectors before flowing into an X-ray exposure cell. SAXS data were collected with 1.5 s exposures at 5 s intervals during elution. The UV absorbance at 280 nm and the LS signals were monitored during chromatography and showed consistent separation of monomeric and dimeric BSA species. Primary data processing is performed using *BioXTAS RAW* (Hopkins *et al.*, 2017) and buffer scattering frames can be extracted for data reduction.

According to the SEC-SAXS data shown in Fig. 6, the BSA samples are heterogenous, with two peaks corresponding to the BSA monomer (R_g = 2.67 nm) and dimer (R_g = 3.47 nm). Therefore, the D_{max} (~11.20 nm) and R_g (~3.02 nm) values calculated via *SAS-cam* are attributed to the heterogeneity of commercially available BSA proteins. The retrieved SAXS model of BSA is superimposed on its atomic structure (PDB entry 3v03; Majorek *et al.*, 2012), showing a good agreement between the two models (Fig. 7).

5. Conclusions and perspectives

SAS-cam is an efficient and user-friendly tool that can be applied to manage, analyse and visualize small-angle X-ray scattering data collected at high-throughput synchrotron beamlines. From the perspective of a general user, *SAS-cam* enables real-time optimization of the sample measurement parameters based on the analysis results. In general, the data processing and output file generation can be done within 2 min for a batch-mode measurement. The fast and interactive data visualization, data reduction and model generation are indispensable for the user to evaluate scattering data quality during an experiment and make quick decisions that yield the best data. The retrieved models are presented as the first round of model reconstruction from SAXS profiles, with the primary aim of providing online feedback. For more sophisticated model reconstructions and cross-validation, sophisticated methods such as *Dammin* (Svergun, 1999), *Gasbor* (Svergun *et al.*, 2001), *DENSS* (Grant, 2018) and *decodeSAXS* (He *et al.*, 2019) are recommended. *SAS-cam* was first deployed on the BioSAXS beamline BL19U2 in 2019. Since then, more than 20 external user groups have collected data on BL19U2 with *SAS-cam* and the feedback has been quite positive with respect to assessment validity, output efficiency and convenience. Users can promptly adjust their experimental plan under the guidance of *SAS-cam* output. Constructive feedback received from beamline users is constantly incorporated into the development of *SAS-cam*. The successful implementation of *SAS-cam* on the BioSAXS beamline BL19U2 helps improve the efficiency of beamline time. Further efforts will be made on the availability of remote computing. The source code can be obtained on request from the authors.

Acknowledgements

The authors thank Alexey Kikhney of the P12 SAXS instrument at EMBL Hamburg Outstation for scientific discussions. We also thank the BL19U2 beamline of the National Facility for Protein Science in Shanghai at the Shanghai Synchrotron Radiation Facility for providing beam study time.

Funding information

The following funding is acknowledged: National Natural Science Foundation of China (grant Nos. U1832144, 31971136 and U1930402); Youth Innovation Promotion Association of the Chinese Academy of Sciences (grant No. 2017319).

References

Blanchet, C. E. & Svergun, D. I. (2013). *Annu. Rev. Phys. Chem.* **64**, 37–54.
Franke, D., Jeffries, C. M. & Svergun, D. I. (2015). *Nat. Methods*, **12**, 419–422.
Franke, D., Petoukhov, M. V., Konarev, P. V., Panjkovich, A., Tuukkanen, A., Mertens, H. D. T., Kikhney, A. G., Hajizadeh, N. R., Franklin, J. M., Jeffries, C. M. & Svergun, D. I. (2017). *J. Appl. Cryst.* **50**, 1212–1225.
Graewert, M. A. & Svergun, D. I. (2013). *Curr. Opin. Struct. Biol.* **23**, 748–754.
Grant, T. D. (2018). *Nat. Methods*, **15**, 191–193.
Guinier, A. & Fournet, G. (1955). *Small Angle Scattering of X-rays.* New York: Wiley.
He, H., Liu, C. & Liu, H. (2019). *iScience*, **23**, 100906.
Hopkins, J. B., Gillilan, R. E. & Skou, S. (2017). *J. Appl. Cryst.* **50**, 1545–1553.

electronic reprint

Hura, G. L., Menon, A. L., Hammel, M., Rambo, R. P., Poole, F. L. II, Tsutakawa, S. E., Jenney, F. E. Jr, Classen, S., Frankel, K. A., Hopkins, R. C., Yang, S., Scott, J. W., Dillard, B. D., Adams, M. W. W. & Tainer, J. A. (2009). *Nat. Methods*, **6**, 606–612.
Jacques, D. A. & Trewhella, J. (2010). *Protein Sci.* **19**, 642–657.
Kikhney, A. G., Borges, C. R., Molodenskiy, D. S., Jeffries, C. M. & Svergun, D. I. (2020). *Protein Sci.* **29**, 66–75.
Kim, T. W., Lee, S. J., Jo, J., Kim, J. G., Ki, H., Kim, C. W., Cho, K. H., Choi, J., Lee, J. H., Wulff, M., Rhee, Y. M. & Ihee, H. (2020). *Proc. Natl Acad. Sci. USA*, **117**, 14996–15005.
Li, N., Li, X., Wang, Y., Liu, G., Zhou, P., Wu, H., Hong, C., Bian, F. & Zhang, R. (2016). *J. Appl. Cryst.* **49**, 1428–1432.
Liu, G., Li, Y., Wu, H., Wu, X., Xu, X., Wang, W., Zhang, R. & Li, N. (2018). *J. Appl. Cryst.* **51**, 1633–1640.
Liu, H., Hexemer, A. & Zwart, P. H. (2012). *J. Appl. Cryst.* **45**, 587–593.
Liu, H. & Zwart, P. H. (2012). *J. Struct. Biol.* **180**, 226–234.
Majorek, K. A., Porebski, P. J., Dayal, A., Zimmerman, M. D., Jablonska, K., Stewart, A. J., Chruszcz, M. & Minor, W. (2012). *Mol. Immunol.* **52**, 174–182.
Nielsen, S. S., Toft, K. N., Snakenborg, D., Jeppesen, M. G., Jacobsen, J. K., Vestergaard, B., Kutter, J. P. & Arleth, L. (2009). *J. Appl. Cryst.* **42**, 959–964.
Pandolfi, R. J., Allan, D. B., Arenholz, E., Barroso-Luque, L., Campbell, S. I., Caswell, T. A., Blair, A., De Carlo, F., Fackler, S., Fournier, A. P., Freychet, G., Fukuto, M., Gürsoy, D., Jiang, Z., Krishnan, H., Kumar, D., Kline, R. J., Li, R., Liman, C., Marchesini, S., Mehta, A., N'Diaye, A. T., Parkinson, D. Y., Parks, H., Pellouchoud, L. A., Perciano, T., Ren, F., Sahoo, S., Strzalka, J., Sunday, D., Tassone, C. J., Ushizima, D., Venkatakrishnan, S., Yager, K. G., Zwart, P., Sethian, J. A. & Hexemer, A. (2018). *J. Synchrotron Rad.* **25**, 1261–1270.
Rodríguez-Ruiz, I., Radajewski, D., Charton, S., Phamvan, N., Brennich, M., Pernot, P., Bonneté, F. & Teychené, S. (2017). *Sensors*, **17**, 1266–1278.
Schilling, M. F. (1990). *Collect. Math. J.* **21**, 196–207.
Svergun, D. I. (1999). *Biophys. J.* **76**, 2879–2886.
Svergun, D. I., Petoukhov, M. V. & Koch, M. H. (2001). *Biophys. J.* **80**, 2946–2953.

electronic reprint